

Size Dependent Phase Diagrams of Nickel-Carbon Nanoparticles

Y. Magnin,¹ A. Zappelli,¹ H. Amara,² F. Ducastelle,² and C. Bichara¹

¹*Centre Interdisciplinaire de Nanoscience de Marseille, Aix-Marseille University and CNRS, Campus de Luminy, Case 913, F-13288 Marseille, France*

²*Laboratoire d'Etude des Microstructures, ONERA-CNRS, BP 72, F-92322 Châtillon, France*

(Received 29 May 2015; published 10 November 2015)

The carbon rich phase diagrams of nickel-carbon nanoparticles, relevant to catalysis and catalytic chemical vapor deposition synthesis of carbon nanotubes, are calculated for system sizes up to about 3 nm (807 Ni atoms). A tight binding model for interatomic interactions drives the grand canonical Monte Carlo simulations used to locate solid, core shell and liquid stability domains, as a function of size, temperature, and carbon chemical potential or concentration. Melting is favored by carbon incorporation from the nanoparticle surface, resulting in a strong relative lowering of the eutectic temperature and a phase diagram topology different from the bulk one. This should lead to a better understanding of the nanotube growth mechanisms.

DOI: 10.1103/PhysRevLett.115.205502

PACS numbers: 61.72.jj, 64.70.Nd, 81.07.De, 81.30.Bx

Reducing dimensions of materials to the nanoscale has a deep impact on their structure and properties. Back in 1976, Buffat and Borel [1] measured a large decrease of the melting temperature of Au nanoparticles (NPs) for sizes down to 2.0 nm. Since then, stimulated by the interest for the synthesis of nanowires and carbon nanotubes by catalytic chemical vapor deposition (CCVD), phase diagrams of alloyed NPs have been actively investigated. Although the smallest catalyst NPs of typical catalysts such as Fe, Co, or Ni are probably liquid under growth conditions [2], the possibility of a synthesis from solid NPs remains open for larger ones and for other less common elements or alloys. Illustrating this dilemma, a route to chiral selective growth of single wall carbon nanotubes (SWNTs) has recently been proposed [3], relying on reportedly solid state NPs, in this instance CoW nanoalloys.

Different from elements of the same group, like Si and Ge that form substitutional alloys with transition metals typically used as catalysts, carbon is smaller and forms interstitial alloys. *In situ* studies are scarce, but subsurface carbon incorporation appears as an important step of the catalytic process for Pd [4] or Ni [5,6]. For Fe, various carbide phases are observed [7], displaying contrasted catalytic activities. It is, therefore, important to understand how carbon incorporation in the catalyst NP, together with its size reduction, modifies its physical and chemical states as compared to the bulk alloy. To address this question, we proceed to establish size dependent nickel-carbon NP phase diagrams in a size range (~1–3 nm) relevant for SWNT growth.

Although not in thermodynamic equilibrium, NPs often have a long enough lifetime to make an experimental determination of their phase diagram possible, usually by transmission electron microscopy (TEM) and structural

investigations. Pt-Ru [8], Au-Ge [9], and Cu-Ni [10] NPs have been studied. In the latter, a phase diagram was established using TEM experiments and CALPHAD type calculations, including interfacial Gibbs energy contributions that become important at the nanoscale. This approach is reported to remain valid for NP diameters down to about 10 nm [11–13]. In the above cited results, the topology of the phase diagrams is preserved even for very small NPs. In such a case, though, Gibb's phase rule [14] might no longer be valid, hence the presence of a eutectic three phase equilibrium should be questioned.

An alternative approach for solving the issues raised by very small NP sizes, is the direct computer simulation of their structure. Density functional theory based molecular dynamics calculations were used for NPs up to 641 atoms [15] to study the size dependent structural changes of icosahedral (I_h) Fe clusters, as well as FePt and CoPt nanoalloys [16]. However, studying binary alloy NPs involves sampling the chemical order. This requires a Monte Carlo simulation approach, associated with simple enough atomic interaction models [17]. Lattice models have been used to study order-disorder phase diagrams of substitutional alloys [18–20], but interstitial alloys such as the metal-carbon systems of interest, here, require considering all degrees of freedom, including atomic relaxations induced by carbon incorporation in interstitial sites. In the framework of carbon nanotube growth, the melting of Fe-C [21] and Ni-C clusters [22] has been studied, but not the states below the liquidus lines. Assuming an equivalence between the NP size reduction and an external pressure increase on the corresponding bulk alloy, Harutyunyan *et al.* [23], predicted a reduced carbon solubility in Fe-C NPs.

In this Letter, we build on our previous studies of carbon solubility in nickel NPs [24,25] to calculate the nickel rich

side of the phase diagram of Ni-C NPs for systems up to 807 Ni atoms, for face centered cubic (fcc, Wulff-shaped) and I_h NPs. We show that, beyond the well-known down shift of the melting points and liquidus lines, the two-phase solid liquid domain of the bulk phase diagram is replaced by a solid core liquid shell domain of the NP that extends to fairly low temperatures. We also evidence qualitative changes in the topology of the phase diagrams, related to the absence of a well-defined eutectic line. We developed an original approach, based on a carefully assessed atomic interaction model for Ni and C, together with computer simulation techniques that have already been discussed in [24,26,27], so that only essential features are recalled here. To describe the Ni-C interactions keeping a quantum mechanical based framework, essential for safe parametrization and transferability, we use a tight binding model that incorporates a moment description of local electronic densities of states at the minimal (fourth moment) level, ensuring a linear scaling of the CPU time with system size. To calculate carbon incorporation in the NPs, with carbon chemical potential (μ_C) as the control variable, we use grand canonical Monte Carlo [28] simulations. Since we focus on carbon solubility in NPs, we checked (see Supplemental Material [29]), that our model correctly reproduces it in bulk systems, with a maximum solubility around 5% at 1865 K. Let us recall that the temperature scale has been reduced by a factor 0.85 to recover the experimental bulk melting temperature of Ni [34].

We studied the phase diagrams of fcc NPs with 201, 405, and 807 Ni atoms in their equilibrium Wulff shape, and also considered icosahedral (I_h) structures with 55, 147, and 309 Ni atoms that present interesting differences. We used and complemented our previous calculations [24], and the convergence of calculations on NPs with 405 and 807 atoms has been reassessed. Computational details, as well as all carbon incorporation isotherms used to calculate the phase diagrams are presented in the Supplemental Material [29]. As observed previously, smaller NPs incorporate larger carbon fractions (x_C) at given μ_C . The role of temperature (T) is similar and the solubility limit slightly increases with T . It is defined as the point in (μ_C , T), and consequently (x_C , T) coordinates, where C atoms start segregating at the surface of the NP. A visual inspection of the NPs shows that increasing μ_C (and consequently x_C) induces a gradual melting of the NPs, that starts on the surface and propagates to the core. Monte Carlo simulations do not yield diffusion coefficients, meaning that amorphous or liquid states cannot be rigorously discriminated. Since we wish to calculate the limits where carbon rich NPs transform into solid, core shell, or homogeneous liquid states, and locate the solubility limits to draw phase diagrams, we need to quantitatively define the molten and crystalline fractions of each NP. This is done using the orientational order parameter first introduced by Steinhardt *et al.* [35], denoted S_i , that enables discriminating solid

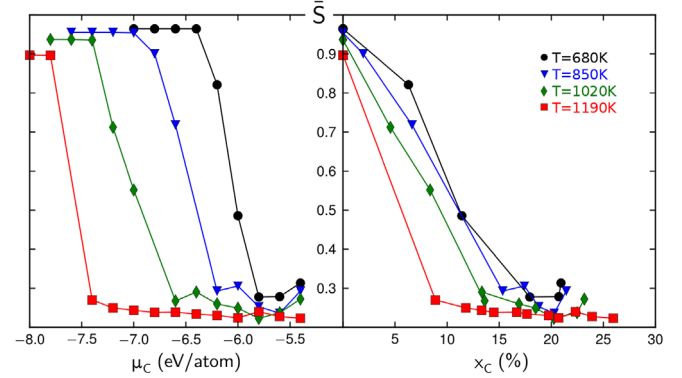


FIG. 1 (color online). Average values of the order parameter (\bar{S}), plotted as a function of μ_C (left) and x_C (right) for a NP, initially icosahedral with 309 Ni atoms, at different temperatures. On the left panel, the solid ($\bar{S} \geq 0.85$) and liquid domains ($\bar{S} \leq 0.35$), separated by a gradual transition zone, are easily identified. The corresponding atomic compositions are readily obtained on the right panel, and a phase diagram can be constructed using the procedure described in [29].

or liquid environments, for each atom i , see [29]. Averaging over all Ni atoms of the NP enables one to assign a global degree of crystallinity to the NP (\bar{S}). It is plotted in Fig. 1 for different temperatures and carbon compositions in the case of the Ni₃₀₉ I_h NP. First, we note that the solid liquid transition is gradual, with a linear dependence of \bar{S} as a function of μ_C . This appears to be a characteristic feature of finite size systems, since in a bulk system, liquid and solid phases should coexist at the same chemical potential. The NP is considered crystalline for $\bar{S} \geq 0.85$, and disordered for $\bar{S} \leq 0.35$. Between these values, solid core molten shell structures prevail. As detailed in [29], plots similar to Fig. 1 are used to locate the transition points and size dependent (x_C , T) phase diagrams are readily obtained.

We start by analyzing the phase diagram of the largest (807 Ni atoms) NP, displayed in Fig. 2. At high T , calculations are easily converged, and homogeneous solid (V) or liquid (I) NPs are identified, as well as a domain (II) where C segregates at the surface of a homogeneous liquid NP, forming chains that are highly mobile, sometimes partly detached from the NP surface. As for a bulk system, the eutectic point (E) of the NP can be taken as the composition (x_E) at the lowest temperature (T_E) of liquid stability. Different from the bulk two phase domain, a solid core liquid shell area (IV) continuously connects solidus and liquidus lines. Visual inspection, as well as the evolution of the order parameter as a function of x_C and T indicate that the liquid outer layer grows continuously at the expense of the solid with increasing carbon content. In the finite sized NP the two phases have to coexist, forming a rather well-defined interface. Within the limits of our calculations that are more difficult to converge at low T , and more difficult to analyze when disorder affects one or two

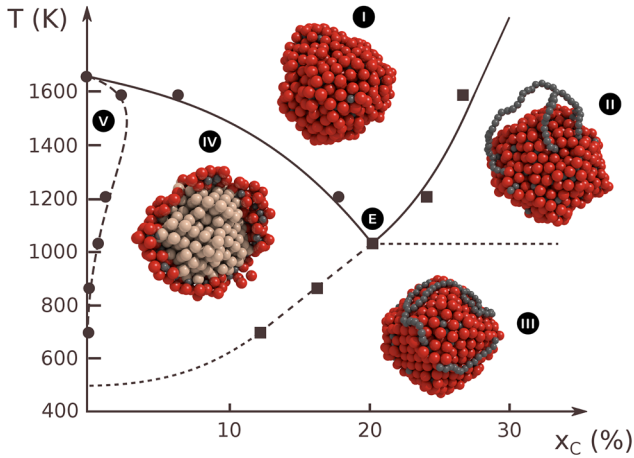


FIG. 2 (color online). Ni-C phase diagram for a NP with 807 Ni atoms. Five domains are identified, illustrated by a snapshot of a characteristic configuration (C atoms: grey, Ni atoms: other colors). I: homogeneous liquid solution; II: C segregation at the surface of liquid NP; III: C segregation from mostly solid NP; IV: solid core liquid shell NP; V: solid solution. The artwork was prepared using Blender [36] and the Atomic Blender add ons.

Ni layers only, core shell structures appear to be present below T_E . Indeed, no sign of a well defined change at T_E could be noticed. Thus, the solubility limit line is extended to lower temperatures. Because of the finite size of the system, interfaces are as important as the homogeneous parts of the system, and the Gibbs phase rule may not apply. This is why a domain (III) is drawn, separated from (II) and (IV) by dashed lines to indicate that the limits are rather fuzzy, where carbon segregation takes place from an essentially solid NP, where disorder is limited to the outermost Ni layer and/or edges or vertices. More details are given in [29]. Let us note that the liquid phase remains stable down to about $x_C \sim 0.21$ and $T \sim 1020$ K, some 700 K below the bulk melting temperature (1728 K). The size reduction has a more dramatic effect on the carbon rich NP than on the pure one. Indeed, as compared to the bulk, the melting temperature of the pure Ni_{807} NP is lowered by $\sim 10\%$, while the eutectic temperature is decreased by $\sim 40\%$. Contrary to the bulk case, though, no evidence for a well-defined isothermal equilibrium line, especially with a crystalline NP, can be found at T_E . On the contrary, an extension of the carbon solubility limit to temperatures below T_E makes sense, since carbon segregation is observed (see [29]) for $x_C < 0.20$, from NPs where facets are still visible, while the outermost layer is disordered. The fairly low temperature (~ 680 K) required to observe C segregation from a faceted and essentially crystalline Ni NP of about 3 nm diameter makes it irrelevant for the selective growth of SWNTs, if we accept the existence of crystalline facets as a key factor to chiral selectivity [3].

We now study the size dependence of the computed phase diagrams and compare them to the experimental bulk

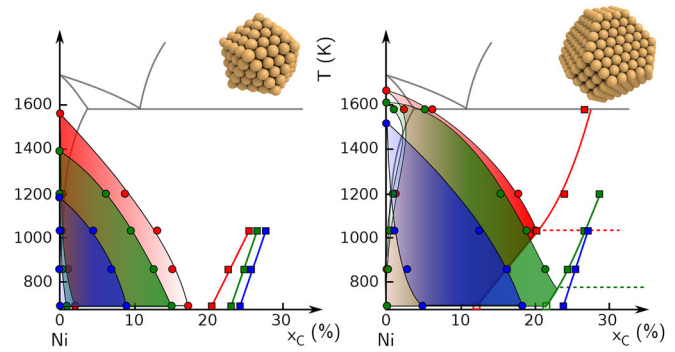


FIG. 3 (color online). Size dependent Ni-C phase diagrams for icosahedral (left) or face centered cubic (Wulff shaped, right) NPs. Full black lines show the bulk phase diagram [37]. Left panel: NPs with 55 (blue), 147 (green), and 309 (red) atoms. Right panel: NPs with 201 (blue), 405 (green), and 807 (red) atoms. For systems smaller than Ni_{405} , the eutectic point, if it exists, is below 680 K.

one [37], as presented in Fig. 3. Initially I_h , with 55, 147, and 309 atoms, and fcc Wulff shaped, with 201, 405, and 807 Ni atom NPs are considered. In the presence of C, the outer layers become topologically disordered, and the difference between I_h and fcc structures gradually washes out. The general trend is that, upon size reduction, the melting points and liquidus lines are shifted to lower temperatures. At constant temperature, the homogeneous liquid domain is larger for smaller NPs because the core shell domain shrinks and carbon solubility limits of liquid NPs are shifted to larger C concentrations. Conversely, this means that, at a given temperature, one needs to reach larger carbon fractions to melt larger NPs. Although determining the solvus lines is difficult, a trend towards an enlargement of the solid state domain with increasing size is observed. Since C incorporation in the interstitial sites of the Ni lattice induces strain, the crystalline structure of smaller NPs is more easily destroyed by inserted C atoms, resulting in a vanishing solid state C solubility. A direct comparison of the solid state solubility limits of I_h and fcc NPs is difficult because sizes do not match and because a complete study should involve not only fcc, I_h , but also decahedral NPs which are very close in terms of stability for small sizes [38]. However, we studied C incorporation in the subsurface of I_h NPs that present both tetrahedral and octahedral interstitial sites. Results, presented in [29], show that, for a given size, octahedral interstitials are more favorable than tetrahedral ones. C incorporation is, thus, easier in Wulff shaped NPs, that have only fcc octahedral interstitial sites and also display (100) facets that are more prone to adsorb and incorporate carbon. Beyond the detailed analysis of the structures, our results call for three general comments.

A key feature of the Ni-C NP phase diagrams is that NP melting is strongly favored by C incorporation, and proceeds from the surface to the core. This is best

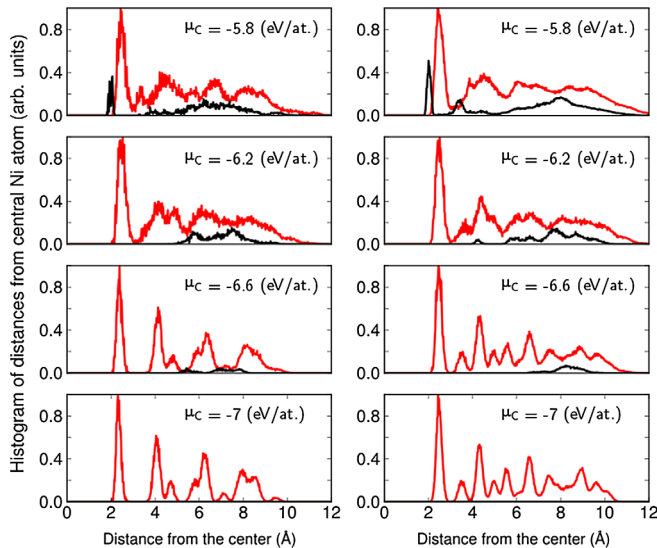


FIG. 4 (color online). Unweighted pair distribution functions (Ni-Ni, red and Ni-C, black) centered on the Ni atom closest to the center of the NP, for a Ni_{309} (left) icosahedral NP and Ni_{405} (right) fcc Wulff-shaped NP calculated at 850 K. The Ni-C distributions have been multiplied by 2 for legibility. Differences in crystalline arrangements of pure NPs are obvious: for $\mu_C = -7.0$ eV/atom: the first peak lies at 0.231 nm for the icosahedral NP while it is 0.013 nm further out for the fcc one, at 0.244 nm, as a result of the larger internal pressure in the former. We clearly see that an outer Ni layer melts for μ_C between -6.6 and -6.2 eV/atom, due to interstitial C incorporation, before full melting at higher μ_C , when C has diffused throughout the NP.

illustrated by the Ni-Ni and Ni-C pair distribution functions, whose evolution as a function of μ_C is presented in Fig. 4 at 850 K for Ni_{309} and Ni_{405} NPs. At low μ_C , no or very few C atoms are incorporated and the crystalline structure of the NP is well preserved. With increasing μ_C , C atoms are incorporated in the outer layers, inducing a gradual melting, characterized by blurred outer Ni layers. This results in a large downshift of the eutectic point, by about 700 K for a Ni_{807} fcc NP, as compared to the bulk phase diagram. Such a behavior might be specific to the Ni-C system where carbon atoms are preferably incorporated in slightly too tight interstitial sites, but other transition metals or alloys might display the same feature.

A second aspect, connected to the melting process, but possibly more general, is the large stability domain of solid core liquid shell NPs that replaces the two-phase solid liquid domain of the bulk phase diagram. While the coexistence of ordered crystalline and disordered (amorphous or liquid) parts of the NP is not that unexpected, the persistence of such core shell structures at temperatures below the eutectic point for small NPs below 3 nm indicates that a bulklike behavior, with an invariant eutectic equilibrium straight line joining the eutectic point and two solid phases is only recovered for larger NPs. Without being able to prove it by calculating a phase diagram for larger NPs,

because of its heavy computing burden, we can easily envision the possibility that the extrapolation of the liquid solubility limit line below the eutectic point, separating domains III and IV in Fig. 2, gradually tends to a horizontal line joining the eutectic point to a solid Ni-rich NP when its size grows bigger.

Finally, turning to a practical application of Ni-C NPs to the synthesis of SWNTs, we see that, in the NP size range spanned here, below 3 nm, the growing tubes are most probably in contact with a liquid or amorphous layer at temperatures relevant for CCVD. In principle, the tube cap nucleation takes place at or beyond the C saturation line, where the outer layer(s) of the NP is (are) disordered. The carbon concentration within this disordered layer depends not only on temperature, but also on its chemical potential (μ_C), determined by the thermochemistry of the decomposition reaction of the carbon feedstock. We know that the contact angle between the Ni-C NP and a growing nanotube depends on the fraction of C dissolved in the NP [25], leading to different growth modes [39]. For low carbon fractions, the Ni NPs tend to wet the C sp^2 walls, so that the growing tube and the NP have essentially the same diameter (tangential growth), while larger carbon fractions lead to dewetting, so that the tube has a smaller diameter than the catalyst NP (perpendicular growth). In addition, related to the possibility of a selective growth of SWNTs from solid NPs, our calculations on Ni indicate that the eutectic temperature is strongly lowered as compared to the bulk one. For the Ni_{807} NP, a homogeneous liquid phase with $\sim 21\%$ C, is stable down to ~ 1020 K, that is $\sim 60\%$ of the bulk melting temperature. If we extrapolate this to another alloy of interest such as the W_6Co_7 compound [3], that melts around 2100 K in the bulk, we see that the question of its physical state (solid, core shell, or liquid) under growth conditions, around 1200 K, remains open. This, of course, depends on the size of the catalyst NP. Thus, we understand how the detailed analysis and predictive evaluation of the state of the catalyst NP, translated in the form of a size dependent phase diagram, can contribute to a better controlled and possibly selective growth of SWNTs.

The research leading to these results has received funding from the European Union Seventh Framework Programme (No. FP7/2007-2013) under Grant No. 604472. The authors also acknowledge support from the French Research Funding Agency (Grant No. ANR-13-BS10-0015-01).

-
- [1] P. Buffat and J.-P. Borel, *Phys. Rev. A* **13**, 2287 (1976).
 - [2] V. Jourdain and C. Bichara, *Carbon* **58**, 2 (2013).
 - [3] F. Yang, X. Wang, D. Zhang, J. Yang, Z. Xu, J. Wei, J.-Q. Wang, Z. Xu, F. Peng, X. Li, R. Li, Y. Li, M. Li, X. Bai, F. Ding, and Y. Li, *Nature (London)* **510**, 522 (2014).

- [4] D. Teschner, J. Borsodi, A. Wootsch, Z. Révay, M. Hävecker, A. Knop-Gericke, S. D. Jackson, and R. Schlögl, *Science* **320**, 86 (2008).
- [5] A. Rinaldi, J.-P. Tessonier, M. E. Schuster, R. Blume, F. Girgsdies, Q. Zhang, T. Jacob, S. B. Abd Hamid, D. S. Su, and R. Schlögl, *Angew. Chem., Int. Ed. Engl.* **50**, 3313 (2011).
- [6] R. S. Weatherup, H. Amara, R. Blume, B. Dlubak, B. C. Bayer, M. Diarra, M. Bahri, A. Cabrero-Vilatela, S. Caneva, P. R. Kidambi, M. Martin, C. Deranlot, P. Seneor, R. Schlögl, F. Ducastelle, C. Bichara, and S. J. Hofmann, *J. Am. Chem. Soc.* **136**, 13698 (2014).
- [7] S. Mazzucco, Y. Wang, M. Tanase, M. Picher, K. Li, Z. Wu, S. Irle, and R. C. J. Sharma, *Catalysis* **319**, 54 (2014).
- [8] C. W. Hills, N. H. Mack, and R. G. Nuzzo, *J. Phys. Chem. B* **107**, 2626 (2003).
- [9] E. Sutter and P. Sutter, *Nano Lett.* **8**, 411 (2008).
- [10] J. Park and J. Lee, *CALPHAD: Comput. Coupling Phase Diagrams Thermochem.* **32**, 135 (2008).
- [11] K. Sim and J. J. Lee, *J. Alloys Compd.* **590**, 140 (2014).
- [12] J. Sopousek, J. Vrestal, J. Pinkas, P. Broz, J. Bursik, A. Styskalik, D. Skoda, O. Zobac, and J. Lee, *CALPHAD: Comput. Coupling Phase Diagrams Thermochem.* **45**, 33 (2014).
- [13] G. Guisbiers, G. Abudukelimu, and D. Hourlier, *Nanoscale Res. Lett.* **6**, 396 (2011).
- [14] M. Hillert, *Phase Equilibria, Phase Diagrams and Phase Transformations* 2nd ed. (Cambridge University Press, Cambridge, England, 2008).
- [15] G. Rollmann, M. E. Gruner, A. Hucht, R. Meyer, P. Entel, M. L. Tiago, and J. R. Chelikowsky, *Phys. Rev. Lett.* **99**, 083402 (2007).
- [16] M. E. Gruner, G. Rollmann, P. Entel, and M. Farle, *Phys. Rev. Lett.* **100**, 087203 (2008).
- [17] F. Baletto and R. Ferrando, *Rev. Mod. Phys.* **77**, 371 (2005).
- [18] J. Pohl, C. Stahl, K. Albe, and J. Beilstein, *Nanotechnology* **3**, 1 (2012).
- [19] D. Alloyeau, C. Ricolleau, C. Mottet, T. Oikawa, C. Langlois, Y. Le Bouar, N. Braidy, and A. Loiseau, *Nat. Mater.* **8**, 940 (2009).
- [20] L. Delfour, J. Creuze, and B. Legrand, *Phys. Rev. Lett.* **103**, 205701 (2009).
- [21] F. Ding, K. Bolton, and A. J. Rosén, *J. Vac. Sci. Technol. A* **22**, 1471 (2004).
- [22] Y. Engelmann, A. Bogaerts, and E. C. Neyts, *Nanoscale* **6**, 11981 (2014).
- [23] A. R. Harutyunyan, N. Awasthi, A. Jiang, W. Setyawan, E. Mora, T. Tokune, K. Bolton, and S. Curtarolo, *Phys. Rev. Lett.* **100**, 195502 (2008).
- [24] M. Diarra, H. Amara, F. Ducastelle, and C. Bichara, *Phys. Status Solidi* **249**, 2629 (2012).
- [25] M. Diarra, A. Zappelli, H. Amara, F. Ducastelle, and C. Bichara, *Phys. Rev. Lett.* **109**, 185501 (2012).
- [26] H. Amara, C. Bichara, and F. Ducastelle, *Phys. Rev. Lett.* **100**, 056105 (2008).
- [27] H. Amara, J.-M. Roussel, C. Bichara, J.-P. Gaspard, and F. Ducastelle, *Phys. Rev. B* **79**, 014109 (2009).
- [28] D. Frenkel and B. Smit, *Understanding Molecular Simulation* (Elsevier, New York, 2002).
- [29] See Supplemental Material at <http://link.aps.org/supplemental/10.1103/PhysRevLett.115.205502> for [brief description], which includes Refs. [30–33].
- [30] M. Moors, H. Amara, T. Visart De Bocarmé, C. Bichara, F. Ducastelle, N. Kruse, and J.-C. Charlier, *ACS Nano* **3**, 511 (2009).
- [31] F.-X. Coudert, M. Jeffroy, A. H. Fuchs, A. Boutin, and C. Mellot-Draznieks, *J. Am. Chem. Soc.* **130**, 14294 (2008).
- [32] S. Jungblut, A. Singraber, and C. Dellago, *Mol. Phys.* **111**, 3527 (2013).
- [33] S. Li, M. S. Sellers, C. Basaran, A. J. Schultz, and D. A. Kofke, *Int. J. Mol. Sci.* **10**, 2798 (2009).
- [34] J. H. Los and R. J.-M. Pellenq, *Phys. Rev. B* **81**, 064112 (2010).
- [35] P. J. Steinhardt, D. R. Nelson, and M. Ronchetti, *Phys. Rev. B* **28**, 784 (1983).
- [36] <http://www.blender.org>.
- [37] V. K. Portnoi, A. V. Leonov, S. N. Mudretsova, and S. A. Fedotov, *Phys. Met. Metallogr. (Transl. of Fiz. Met. Metalloved.)* **109**, 153 (2010).
- [38] C. Mottet, J. Goniakowski, F. Baletto, R. Ferrando, and G. Tréglia, *Phase Transit.*, **77**, 101 (2004); **77**, 101 (2004).
- [39] M.-F. C. Fiawoo, A.-M. Bonnot, H. Amara, C. Bichara, J. Thibault-Pénisson, and A. Loiseau, *Phys. Rev. Lett.* **108**, 195503 (2012).